Chapter 9
Optimal Placement of Reactive Power Compensators in AC Power Network

Hossein Shayeghi and Yashar Hashemi

Abstract A framework and versatile approach is presented in this chapter to extend a multi-objective reactive power planning (RPP) method for concurrently study of reactive power from flexible alternating current transmission system (FACTS) devices and capacitor banks. The proposed plan will enable system operators to define the optimal location of FACTS devices and capacitor banks that should be connected in the network to improve voltage stability, active power losses and the cost of VAR injection. A formulation and solution method are presented for the RPP problem, including FACTS devices and capacitor banks.

Nomenclature

FDM	Fuzzy decision making	NTVE	Nonlinear time-varying evolution
RPP	Reactive power planning	Z_{shi}, Z_{sein}	Shunt and series transformer impedances
FACTS	Flexible ac transmission system	V_{shi}, V_{sein}	Injected voltage of M-FACT
MO	Multi-objective	$\Delta P_{g,j}$	The change in the plan of the jth generator
SLP	Sequential linear programming	$x_i(k)$	Situation of ith particle at iteration k
MILP	Mixed integer linear programming	$x_i^l(k)$	Local best of ith particle at iteration k
OPF	Optimal power flow	x^g	Global best of all particles
SVC	Static VAR compensator	$v_i(k)$	Velocity of ith particle at iteration k

(continued)

H. Shayeghi (✉) · Y. Hashemi
Technical Engineering Department, University of Mohaghegh Ardabili, Ardabil, Iran
e-mail: hshayeghi@gmail.com

Y. Hashemi
e-mail: yashar_hshm@yahoo.com

N. Mahdavi Tabatabaei et al. (eds.), *Reactive Power Control in AC Power Systems*, Power Systems, DOI 10.1007/978-3-319-51118-4_9

(continued)

STATCOM	Static synchronous compensator	c_1	Cognitive parameter (acceleration coefficient)
TCSC	Thyristor controlled series compensator	c_2	Social parameter (acceleration coefficient)
UPFC	Unified power flow controller	ϕ_1, ϕ_2	Random numbers between 0 and 1
PST	Phase-shifting transformer	S_{iSC}, S_{iHFC}	Size related to the ith HFC and slow VAR device
MSC	Mechanically-switched shunt capacitor	k_S, k_R	Stator and rotor leakage factor
TSSC	Thyristor switched series capacitor	Q_{GSC}	Reactive power injected from GSR
TSSR	Thyristor switched series reactor	S_{GSC}	Apparent power of GSC
DM	Decision makers	k_L, k_C	The amount of X_C and X_L in service
HFC	Hybrid flow controller	C_{iHFC}, C_{iSC}	Cost function of the ith HFC and slow VAR device
M-FACTS	Multi-converter FACTS	k	PST voltage ratio
MOP	Multi-objective problem	r_T	Discount rate
MOPSO-NTVE	Multi-objective particle swarm optimization		

9.1 Introduction

Reactive power planning includes all management actions to improve the voltage profile, voltage stability and other objectives. Recent researches have represented optimization-based techniques to verify RPP issue. RPP problem is one of the most challenging issues in power system studies. Current costs such as variable and fixed VAR set up cost, power loss cost, and fuel cost may be used for target function of RPP [1]. Other targets may be deviation from a given plan of a control parameter (such as voltage) or voltage stability margin that is used as a multi-objective (MO) model [2]. Several network blackouts related to deficiency of reactive power in stiffly stressed situations have shown that voltage collapse issue is closely related to reactive power handling [3]. Thus, the main purpose of the RPP problem is to obtain minimum investment cost in new reactive plan which is necessary to preserve acceptable voltage profiles [4].

Power grids are stressed due to various causes; high cost of extending transmission lines, difficulty of getting right of way, and change in generating schemes related to pecuniary and environmental concerns, and enlarged loading of transmission grid. These issues have infused power utilities to discuss maintaining

against voltage instability as an essential option in reactive power planning. Hence, the coordinated VAR management plan can be verified as specifying reactive power expansion plan that convinces requirements for voltage deviation and voltage permanency. This issue makes a great non-linear optimization subject.

Different methods are used to solve RPP problem. Sequential linear programming (SLP) was reported for VAR management and pricing in [5]. Other procedures have considered integer parameters to shape discrete scales and fixed costs, mainly based on Benders decomposition [6]. This technique mixes use of mixed integer linear programming (MILP) for finance sub-problem and classical optimal power flow (OPF) for operational sub-problem.

Reactive power management has gained more importance due to the inclusion of FACTS devices in transmission networks in the system [7]. Optimal allocation of fast reactive power tools, as for example static VAR compensator (SVC) [8], static synchronous compensator (STATCOM), static inter-phase power controller (SIPC) [9], thyristor controlled series compensator (TCSC) and unified power flow controller (UPFC), is a critical component in RPP problem solution or VAR management. Hybrid flow controller (HFC) is a novel FACTS device that is constructed from a conventional phase-shifting transformer (PST), a mechanically-switched shunt capacitor (MSC), a multi-module thyristor switched series capacitor (TSSC) and a multi-module thyristor switched series reactor (TSSR) [10].

With regard to property of series and shunt compensation in HFC structure, its function is similar to UPFC. Since HFC has some preference than the UPFC, it is expected that application of this device would be expanded. Cost efficiency of HFC is better than UPFC [11]. In [12], it was indicated that HFC may be used for the most effective satisfaction of dispatcher demand supported technical and economic characteristics. Simplicity of idea, management and operational ways, lower loss and higher efficiency are the advantages of HFC. Furthermore, HFC produces low harmonics and has no incompatible result on power quality index.

There are many structures by combining two or more converter blocks. Interline power flow controller (IPFC), the generalized unified power flow controller (GUPFC) and generalized interline power flow controller (GIPFC) are developed to regulate power flows of sub-grid rather than regulate power flow of single line by a UPFC or static synchronous series compensator (SSSC). The suitable control ability of the multi-converter FACTS (M-FACTS) presents an excellent potential in solving several problems in electric utilities [13]. The optimal power flow with the M-FACTS devices would be an effective tool to control, plan and manage power network [14].

9.1.1 Objectives

A framework for deriving FACTS steady state studies based on injection models is presented. The presented framework has the following specifications:

- Active and reactive power is applied as management parameters. It's a suitable technique which models nearly any kind of FATCS tools. In this model, FACTS control parameters are the injected powers.
- In this model, the injected power is an independent index that does not change with the amplitudes and phases of linked node voltage. In this case the Jacobian matrix does not vary within power flow iterations.
- Since in the model built, power injections are treated as values, which do not vary with the connected node voltage, thereby the need not to be modified during the. Thus, it is easy and efficient to implement.

In this chapter the injection model of FACTS devices is used to investigate its effect on power flow of the power system. At first, the injection pattern of FACTS tools is extracted. Then, a steady state study is defined by FACTS devices injection pattern. To find size and site of FACTS tools, a multi-objective optimization procedure is developed for decreasing the overall costs of RPP and improving voltage behavior of the power network. Multiple objectives are considered at the same time which addresses the multi-objective design technique. In a case that FACTS devices are connected in a power grid, its cost should be considered that it is related to the converter capacity. The purpose of RPP is to prepare adequate VAR sources for the system to be acted economically. The aims of VAR design issues contain decreasing investment cost and voltage deviation, and voltage stability criterion maximization.

In multi-target issues the objectives are in contrast with each other. Thus, a set of solutions is obtained instead of one. In this work, multi-objective optimization algorithms are used to get the non-dominated set. This survey implements an external archive to retain all non-dominated sets within the evolutionary procedure and a fuzzy decision-making technique is used to group these solutions based on their significance. Decision makers can choose the suitable solution among them by utilizing the fuzzy decision-making manner. Applying a multi-target optimization method is an appropriate method to plan and to placement reactive power tools by considering simultaneously an extensive range of target functions such as: correcting the voltage stability, power losses reduction or decreasing the cost of VAR sources.

The presented procedure is applied on IEEE 57 bus power grid to illustrate the optimal operation of power network and the achieved outcomes are compared. Two new FACTS devices, HFC and M-FACTS, are discussed in this chapter.

The chapter is organized into 5 sections. The second section verifies FACTS devices and their use in the intent of RPP and operational subjects with power flow issues. The overall aims and objectives of the FACTS technology are achieved in Sect. 9.2. This section reviews the steady condition behaviors of the transmission lines. Also, it contains the analysis of FACTS controller on power flow and voltage profile. Section 9.2 covers the modeling of the various FACTS devises, HFC and GUPFC. The second section presents the modeling and steady state characteristics of HFC and GUPFC. In each case of FACTS devices, the action of the FACTS tools is clarified with the explanation of the power circuit, associated controllers and

operating modes. The idea of the application of multi-objective optimization method in achieving the desired level of techno-economic share of FACTS devices in power grid action and RPP issue is given in two Sects. 9.3 and 9.4. In these sections to extract size and site of FACTS tools and capacitor banks, multi-objective optimization algorithm based on multi-attribute decision making method is developed by formulating the overall costs of power generation and maximizing of profit. The method of investment analysis and the allocation process of FACTS devices in power network are explained in Sect. 9.5. Section 9.5 provides the test network. Simulation outcomes of the presented technique and conclusion remarks are presented in Sect. 9.5.

9.2 Steady State Characteristics of the FACTS Devices

9.2.1 Hybrid Flow Controller

The power injection model of [12] is used to model HFC. This model of HFC is suitable for conventional power flow analysis. The accuracy and the conformability of this model on any power system leads to accurate steady state analysis. The structure of the HFC has been given in Fig. 9.1. V_i and V_j are voltage phasors of buses i, j, respectively. The PST induces voltage V_P and V_i' is the voltage of the HFC internal node. Magnitude of V_{XC} and V_{XL} depend on value of line flow I_{ij} and the number of TSSC and TSSR units. The series injected voltage of PST and the limitation proposing power interchange between transformers of the PST, can be explained as follows equations

$$V_P = jkV_E \tag{9.1}$$

$$V_E = V_i - jX_E I_E \tag{9.2}$$

$$V_P I_{ij}^* = V_E I_E^* \tag{9.3}$$

where, k is the PST voltage proportion and X_E is the leakage reactance related to excitation transformer. Substituting (9.1) in (9.3), we obtain

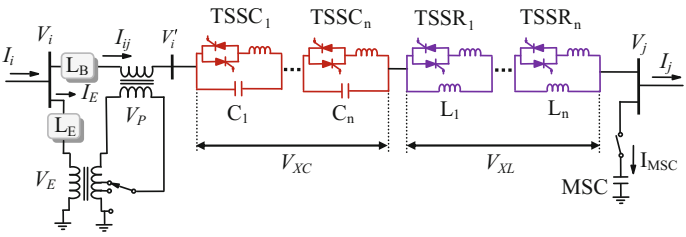

Fig. 9.1 Schematic diagram of HFC

$$I_E = -jkI_{ij} \tag{9.4}$$

The line current I_{ij} is as follows

$$I_{ij} = \frac{(1+jk)V_i - V_j}{j(k_L X_L + k^2 X_E + X_B - k_C X_C)} \tag{9.5}$$

where, k_L and k_C are the amount of X_C and X_L in service and X_B is the leakage reactance of series transformer. The currents I_i and I_j based on V_i and V_j is developed as follows:

$$I_i = \frac{\left((1+k^2)V_i - (1-jk)V_j\right)}{j(k_L X_L + k^2 X_E + X_B - k_C X_C + X_S)} \tag{9.6}$$

$$I_j = \frac{\left((1+jk)V_i - V_j\right)}{j(k_L X_L + k^2 X_E + X_B - k_C X_C + X_S)} + \frac{V_j}{jX_{MSC}} \tag{9.7}$$

If the current I_B be expressed as

$$I_B = \frac{V_i - V_j}{jX_B} \tag{9.8}$$

The injected current into bus i is as follows

$$I_{SS} = I_B - I_i = \frac{\left((1+k^2)V_i - (1-jk)V_j\right)}{j(k_L X_L + k^2 X_E + X_B - k_C X_C + X_S)} + \frac{\left(-V_i + V_j\right)}{jX_B} \tag{9.9}$$

The active and reactive power P_{SS} and Q_{SS} injected by I_{SS} into bus i are written as

$$P_{SS} = -\frac{|V_i||V_j|\left(k\cos(\theta_i - \theta_j) + \sin(\theta_i - \theta_j)\right)}{(k_L X_L + k^2 X_E + X_B - k_C X_C + X_S)} + \frac{|V_i||V_j|}{X_B}\sin(\theta_i - \theta_j) \tag{9.10}$$

$$\begin{aligned} Q_{SS} = &-\frac{|V_i|\left(|V_i|(1+k^2) + k|V_j|\sin(\theta_i - \theta_j) - |V_j|\cos(\theta_i - \theta_j)\right)}{(k_L X_L + k^2 X_E + X_B - k_C X_C + X_S)} \\ &+ \frac{|V_i|}{X_B}\left(|V_i| - |V_j|\cos(\theta_i - \theta_j)\right) \end{aligned} \tag{9.11}$$

The injected current into bus j can be determined as follows

$$\begin{aligned} I_{SR} = I_j - I_B = &\frac{\left((1+jk)V_i - V_j\right)}{j(k_L X_L + k^2 X_E + X_B - k_C X_C + X_S)} \\ &+ \frac{\left(-V_i + V_j\right)}{jX_B} + \frac{V_j}{jX_{MSC}} \end{aligned} \tag{9.12}$$

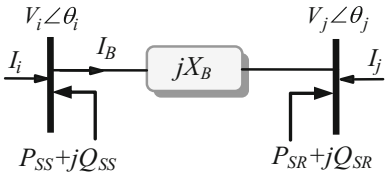

Fig. 9.2 Injection model for HFC

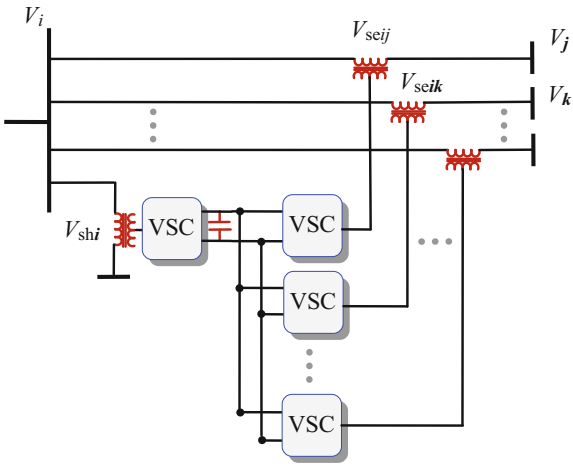

Fig. 9.3 M-FACTS structure with a shunt converter and several series converter

According to Fig. 9.2 the active and reactive power injected by I_{SR} into bus j are as

$$P_{SR} = -P_{SS} \tag{9.13}$$

$$\begin{aligned} Q_{SR} = &-\frac{|V_i|\left(|V_i|\cos(\theta_i-\theta_j)-k|V_j|\sin(\theta_i-\theta_j)-|V_j|\right)}{(k_L X_L + k^2 X_E + X_B - k_C X_C + X_S)} \\ &+\frac{|V_j|\left(|V_j|-|V_i|\cos(\theta_i-\theta_j)\right)}{X_B}+\frac{k_m|V_j|^2}{X_{MSC}} \end{aligned} \tag{9.14}$$

9.2.2 *Multi-converter FACTS Devices*

The principle aim of the M-FACTS is to adjust the voltage and power flow [15]. The circuit of the M-FACTS including of a shunt injected voltage source and two series injected voltage sources is given in Figs. 9.3 and 9.4. Active power can be interchanged among these converters based on the DC branch. In M-FACTS with one shunt converter and two series converters, it can adjust five power grid parameters such as node voltage and active and reactive power of two lines.

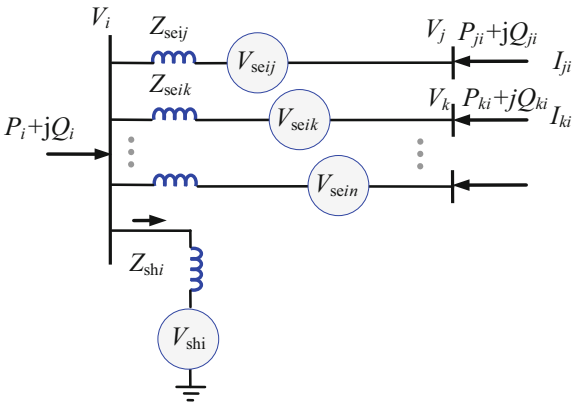

Fig. 9.4 M-FACTS diagram with a shunt converter and several series converters

More series converters can present more degrees of control. The Z_{shi} and Z_{sein} in Fig. 9.4 are shunt and series transformer impedances. The injected voltage sources that are shown in Fig. 9.2 are explained as follows:

$$V_{shi} = V_{shi}\angle\theta_{shi} \tag{9.15}$$

$$V_{sein} = V_{sein}\angle\theta_{sein} \tag{9.16}$$

where V_{shi}, V_{sein} are injected voltage of M-FACTS and $n = j, k, \ldots$.

9.2.2.1 Power Flow Equations of M-FACTS

As shown in Fig. 9.4, the power flow relations of M-FACTS can be given as

$$\begin{aligned} P_i = {} & V_i^2 g_{ii} - V_i V_{shi}(g_{shi}\cos(\theta_i - \theta_{shi}) + b_{shi}\sin(\theta_i - \theta_{shi})) \\ & - \sum_n V_i V_n (g_{in}\cos\theta_{in} + b_{in}\sin\theta_{in}) \\ & - \sum_n V_i V_{sein}(g_{in}\cos(\theta_i - \theta_{sein}) + b_{in}\sin(\theta_i - \theta_{sein})) \end{aligned} \tag{9.17}$$

$$\begin{aligned} Q_i = {} & -V_i^2 b_{ii} - V_i V_{shi}(g_{shi}\sin(\theta_i - \theta_{shi}) + b_{shi}\sin(\theta_i - \theta_{shi})) \\ & - \sum_n V_i V_n (g_{in}\sin\theta_{in} - b_{in}\cos\theta_{in}) \\ & - \sum_n V_i V_{sein}(g_{in}\sin(\theta_i - \theta_{sein}) - b_{in}\cos(\theta_i - \theta_{sein})) \end{aligned} \tag{9.18}$$

$$\begin{aligned} P_{ni} = {} & V_n^2 g_{nn} - V_i V_n (g_{in}\cos(\theta_n - \theta_i) + b_{in}\sin(\theta_n - \theta_i)) \\ & V_n V_{sein}(g_{in}\cos(\theta_n - \theta_{sein}) + b_{in}\sin(\theta_n - \theta_{sein})) \end{aligned} \tag{9.19}$$

$$\begin{aligned} Q_{ni} &= -V_n^2 b_{nn} - V_i V_n \left(g_{in}\sin(\theta_n - \theta_i) - b_{ij}\cos(\theta_n - \theta_i)\right) \\ & V_n V_{sein}(g_{in}\cos(\theta_n - \theta_{sein}) - b_{in}\cos(\theta_n - \theta_{sein})) \end{aligned} \tag{9.20}$$

where $g_{shi} + jb_{shi} = 1/Z_{shi}$, $g_{in} + jb_{in} = 1/Z_{sein}$, $g_{nn} + jb_{nn} = 1/Z_n$, $g_{ii} = g_{shi} + \sum_n g_{in}$, $b_{ii} = b_{shi} + \sum_n b_{in}$, and $n = j, k, \ldots$

9.2.2.2 Operating Limitations of M-FACTS

Active power change in DC branch based on operating limitations among converters is as follows:

$$PE = \mathrm{Re}\left(V_{shi} I_{shi}^* - \sum_n V_{sein} I_{ni}^*\right) = 0 \tag{9.21}$$

or

$$\begin{aligned} PE = {} & V_{shi}^2 g_{shi} - V_i V_{shi}(g_{shi}\cos(\theta_i - \theta_{shi}) - b_{shi}\sin(\theta_i - \theta_{shi})) \\ & + \sum_n \left(V_{sein}^2 g_{in} - V_i V_{sein}(g_{in}\cos(\theta_i - \theta_{sein}) - b_{in}\sin(\theta_i - \theta_{sein}))\right) \\ & + \sum V_n V_{sein}(g_{in}\cos(\theta_n - \theta_{sein}) - b_{in}\sin(\theta_n - \theta_{sein})) = 0 \end{aligned} \tag{9.22}$$

where $n = j, k, \ldots$. The related injected voltage source bound limitations

$$\begin{aligned} V_{shi}^{\min} &\le V_{shi} \le V_{shi}^{\max} \\ \theta_{shi}^{\min} &\le \theta_{shi} \le \theta_{shi}^{\max} \\ V_{sei}^{\min} &\le V_{sei} \le V_{sei}^{\max} \\ \theta_{sei}^{\min} &\le \theta_{sei} \le \theta_{sei}^{\max} \end{aligned}$$

where $n = j, k, \ldots$

9.2.2.3 Injection Pattern of GUPFC

In general, GUPFC consist three voltage source converters and using this basic configuration, it can adjust simultaneously power flow in two transmission lines by varying device control parameters. For the sake of explanation, the complete voltage source-based mathematical modeling of GUPFC is presented in this section. The principle configuration of GUPFC linked between nodes i, j and k is illustrated in Fig. 9.5.

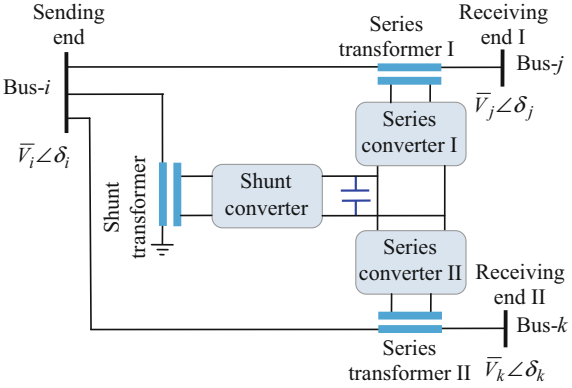

Fig. 9.5 Schematic diagram of GUPFC

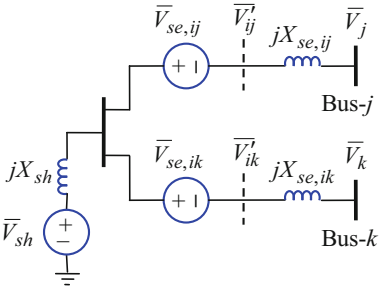

Fig. 9.6 Voltage source model of GUPFC

In this configuration, two voltage source converters are connected in two different transmission lines having a common bus. The third converter is connected at this common bus and acts as a shunt connected voltage source converter. This shunt converter supplies the power that is supplied by the series converters. All these converters are linked through a common DC branch to exchange the power flow. For the sake of simplification, it is assumed that, the voltage injected by the series converters is sinusoidal and the reactance of the coupling transformer is neglected. With these assumptions, the final voltage source plan of GUPFC is exhibited in Fig. 9.6. The voltages at GUPFC connected buses can be expressed as

$$V_m = |V_m|\angle\delta_m \quad \forall \; m = i, j, k \tag{9.23}$$

The applied voltage of the series converters can be represented as:

$$V_m = |V_m|\angle\delta_m \quad \forall \; m = i, j, k \tag{9.24}$$

In Fig. 9.2, the voltage behind the series voltage source can be expressed for both converters as:

$$\overline{V}'_{im} = \overline{V}_i + \overline{V}_{se,im} \quad \forall \; m = j, k \tag{9.25}$$

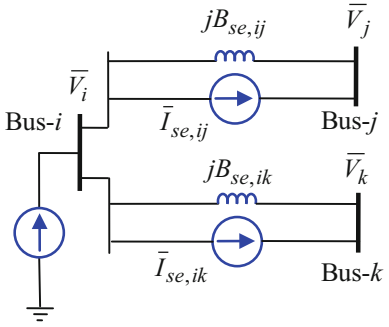

Fig. 9.7 Equivalent current source model GUPFC

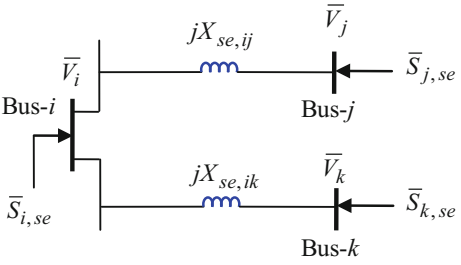

Fig. 9.8 Voltage source model of GUPFC

To develop the injection pattern, the voltage source exhibition is converted into an equivalent current source model using Norton's theorem and is shown in Fig. 9.7.

$$I_{se,im} = -jB_{se,im}\overline{V}_{se,im} \tag{9.26}$$

where $B_{se,im} = 1/jX_{se,im}$ is the admittance of the coupling transformer.

Using this, the power injected by these sources at the device connected buses can be expressed as

$$S_{i,se} = \overline{V}_i(-\overline{I}_{se,ij} - \overline{I}_{se,ik})^* \tag{9.27}$$

$$S_{m,se} = \overline{V}_m\overline{I}^*_{se,im} \tag{9.28}$$

Using Eqs. (9.4), (9.5) and (9.6) can be simplified as:

$$\overline{S}_{i,se} = \sum_{m=j,k}(-jV_iV_{se,im}B_{se,im}\angle(\delta_i - \theta_{se,im})) \tag{9.29}$$

$$\overline{S}_{m,se} = jV_mV_{se,im}B_{se,im}\angle(\delta_m - \theta_{se,im}) \quad \forall \ m = j,k \tag{9.30}$$

The final series voltage source with the related power injections is illustrated in Fig. 9.8.

Similarly, the shunt VSC can be modeled as a power injection pattern at the respective bus. In this modeling, it is assumed that, the reactive power applied by

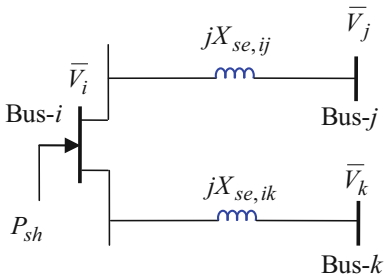

Fig. 9.9 Equivalent shunt voltage source pattern

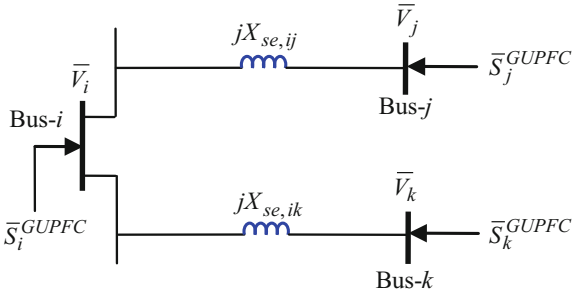

Fig. 9.10 Equivalent power injection model of GUPFC

the shunt VSC is zero, because the purpose of this reactive power is to preserve the voltage value at the converter connected node. The equivalent shunt voltage source pattern of GUPFC is illustrated in Fig. 9.9. The net active power applied at shunt converter connected bus can be expressed as:

$$P_{sh} = -P_{series,ij} - P_{series,ik} \tag{9.31}$$

The magnitude of the apparent power of series converters can be calculated as:

$$\overline{S}_{series,im} = \overline{V}_{se,im} I_{ij}^{*} = j\overline{V}_{se,im} B_{se,im} (\overline{V'}_{ij} - \overline{V}_m)^{*} \quad \forall \ m = j,k \tag{9.32}$$

Using Eq. (9.32), after simplifying, the expressions for active and reactive powers supplied by the series converters derived are

$$\begin{aligned} P_{series,im} &= V_i V_{se,im} B_{se,im} \sin(\theta_{se,im} - \delta_i) \\ &\quad - V_m V_{se,im} B_{se,im} \sin(\theta_{se,im} - \delta_j) \quad \forall m = j,k \\ Q_{series,im} &= -V_i V_{se,im} B_{se,im} \cos(\theta_{se,im} - \delta_i) \\ &\quad + V_m V_{se,im} B_{se,im} \cos(\theta_{se,im} - \delta_j) - V_{se,ij}^2 B_{se,ij} \quad \forall \ m = j,k \end{aligned} \tag{9.33}$$

The final power injection pattern is obtained by combining series voltage source pattern and shunt voltage source model. The combined model is displayed in Fig. 9.10. The respective power injections at GUPFC connected buses can be obtained as

$$\begin{aligned}
P_i^{GUPFC} &= 2V_iV_{se,ij}B_{se,ij}\sin(\delta_i-\theta_{se,ij})+2V_iV_{se,ik}B_{se,ik}\sin(\delta_i-\theta_{se,ik})\\
&\quad -V_iV_{se,ij}B_{se,ij}\sin(\delta_i-\theta_{se,ij})-V_iV_{se,ik}B_{se,ik}\sin(\delta_i-\theta_{se,ik})\\
Q_i^{GUPFC} &= -V_iV_{se,ij}B_{se,ij}\sin(\delta_i-\theta_{se,ij})-V_iV_{se,ik}B_{se,ik}\sin(\delta_i-\theta_{se,ik})\\
P_j^{GUPFC} &= -V_jV_{se,ij}B_{se,ij}\sin(\delta_j-\theta_{se,ij})\\
Q_j^{GUPFC} &= V_jV_{se,ij}B_{se,ij}\cos(\delta_j-\theta_{se,ij})\\
P_k^{GUPFC} &= -V_kV_{se,ik}B_{se,ik}\sin(\delta_k-\theta_{se,ik})\\
Q_k^{GUPFC} &= V_kV_{se,ik}B_{se,ik}\cos(\delta_k-\theta_{se,ik})
\end{aligned} \tag{9.34}$$

9.3 RPP by VAR Resources

The VAR management problem is the determination of an action and provision of new reactive tools that minimize RPP cost (*INV*), voltage deviation (V_D) and STC-criterion (STC).

RPP cost (INV): The first target function includes two sections. The first section determines the overall cost of energy loss (EL_C) as bellow:

$$EL_C = 24\times 365\times hP_{loss} \tag{9.35}$$

where h is per-unit energy cost (0.06 $/KWh). The power loss in transmission branches can be given as follows

$$P_{loss}=\sum_{k=1}^{n_l} g_k\left[V_i^2+V_j^2-2V_iV_j\cos\left(\delta_i-\delta_j\right)\right] \tag{9.36}$$

The cost of the new prepared VAR tools is systematized as the total investment cost of VAR device, as OC_{var}

$$OC_{var}=\frac{r_T(r_T+1)^{n_T}}{(1+r_T)^{n_T}-1}\times\sum_{i\in\Omega}\left(C_{iFACTS}S_{iFACTS}+C_{iSC}S_{iSC}\right) \tag{9.37}$$

where, C_{iFACTS} and C_{iSC} are the cost function of the ith FACTS and slow VAR device. S_{iFACTS} and S_{iSC} refer to size related to them and Ω is the set of all candidate locations. For long-term cost analysis, it is necessary to consider the lifetime and discount rate as n_T and r_T, respectively. The cost function of the HFC, M-FACTS and slow VAR device can be represented in a quadratic form [16, 17]

$$C_{i,HFC}=0.00012\,S_{i,HFC}^2-0.10764\,S_{i,HFC}+75.288 \tag{9.38}$$

$$C_{i,SC}=0.000000014\,S_{i,SC}^3-0.0000014\,S_{i,SC}^2+0.0052\,S_{i,SC}+0.91 \tag{9.39}$$

$$C_{M-FACTS} = 0.00045\, S^2_{M-FACTS} - 0.40365\, S_{M-FACTS} + 282.33 \tag{9.40}$$

where S_{iSC}, S_{iHFC} are size related to the ith HFC. Thus, the overall cost can be presented as the sum of two costs as OC_{var} and EL_C. The annual cost is calculated as follows

$$INV = \min(OC_{var} + EL_C) \tag{9.41}$$

Voltage deviation (V_D): This target is to optimize the voltage magnitude variations at load nodes that can be presented by

$$V_D = \min\left\{\sum_{k=1}^{N_L} |V_K - 1|\right\} \tag{9.42}$$

where, N_L is the number of load nodes.

STC criterion (STC): This aim is to optimize the index for defining the voltage stability of the system and is given by [18]

$$STC = \min\left\{\max_{j\in N_L}(STC_j)\right\} \tag{9.43}$$

Equation (9.43) requires finding the magnitude for STC_j in total load buses. After determining all magnitudes of STC_j, the load node which has the maximum STC_j is found. The definition of STC_j among total load buses has been presented by Eq. (9.44). One method of determining STC is

$$STC = \min\left\{\max_{j\in N_L}\left|\frac{V_j - \sum_{i\in N_G} H_{ji}V_i}{V_j}\right|\right\} \tag{9.44}$$

The magnitudes of H_{ji} are received from the H_{LG} matrix as follows

$$H_{LG} = -[Y_{LL}]^{-1}[Y_{LG}] \tag{9.45}$$

where, Y_{LL} and Y_{LG} are separated sections of grid Y-bus matrix. The elements of H_{LG} matrix are complex and its columns related to the generator node numbers and rows related to the load node numbers. This matrix presents the data for each load node about the value of power that should be given from each generator in the normal and grid contingencies as far as the system efficiency is assumed based on voltage profiles. To guarantee the stability situation, the state of $STC_j \leq 1$ must not be deviated for any of the jth node.

9.4 MOPSO-NTVE Algorithm Implementation to Solve RPP Problem

Multi-objective optimization: To determine the collection of solutions related to the multi-target problem, Pareto optimality idea is applied [19]. The total multi-target optimization issue, without limitations, can be presented as bellow [20]

$$\min f(x) = (f_1(x), f_2(x), \ldots, f_m(x)) \tag{9.46}$$

where $x \in \Omega$ is a possible solution set, Ω is the possible area of the problem, m is the number of targets and $f_i(x)$ is the ith target function of the matter. The aim is to optimize m target functions concurrently, to determine a suitable trade-off of solutions that present the best agreement among the objectives. So, assuming $f(x) = (f_1(x), f_2(x), \ldots, f_m(x))$ and $f(y) = (f_1(y), f_2(y), \ldots, f_m(y))$, $f(x)$ dominates $f(y)$, denoted by $f(x) < f(y)$, if and only if (minimization) [21]:

$$\begin{aligned} &\forall i \in \{1, 2, \ldots, m\} : f_i(x) \leq f_i(y) \\ &\exists i \in \{1, 2, \ldots, m\} : f_i(x) < f_i(y) \end{aligned} \tag{9.47}$$

If there is no $f(y)$ that dominates $f(x)$, $f(x)$ is non-dominated. Moreover, if there is no solution y that dominates x, x is defined Pareto optimal and $f(x)$ is a non-dominated purpose vector. The Pareto optimal set is signified by P^*, and the collection of total non-dominated target vector is defined Pareto front, signified by PF^*.

Multi-objective particle swarm optimization method with nonlinear time-varying evolution (MOPSO-NTVE): The position and the velocity of the ith individual in the n-dimensional search region is verified as $x_i = [x_{i,1} \quad x_{i,2} \quad \ldots \quad x_{i,n}]$ and $v_i = [v_{i,1} \quad v_{i,2} \quad \ldots \quad v_{i,n}]$, respectively where $v_i(k)$ is velocity of ith particle at iteration k and $x_i(k)$ is situation of ith particle at iteration k. The local best of the ith individual is defined as $x_i^l = [x_{i,1}^l \quad x_{i,2}^l \quad \cdots \quad x_{i,n}^l]$ and the global best determined so far explained as $x^g = [x_1^g \quad x_2^g \quad \cdots \quad x_n^g]$. At each iteration, the new velocities of the individuals are updated by employing the given equation:

$$\begin{aligned} v_i(k+1) = C(\phi)\{&\omega(k) v_i(k) + c_1(k)\varphi_1(x_i^l(k) - x_i(k)) \\ &+ c_2(k)\varphi_2(x^g(k) - x_i(k))\} \quad \text{for} \quad i = 1, 2, \ldots, m \end{aligned} \tag{9.48}$$

The first section illustrates the current velocity of the individual, second section represents the cognitive term of MOPSO-NTVE and the third section related to the social term of MOPSO-NTVE. Each individual moves from the current condition to the next one by the changed velocity as bellow

$$x_i(k+1) = x_i(k) + v_i\,(k+1) \quad \text{for} \;\; i = 1, 2, \ldots, m \tag{9.49}$$

where m and k are number of individuals and current iteration, $x_i(k)$ is the situation of ith individual at iteration k, $x_i^l(k)$ and x^g are local and global best, $v_i(k)$ is velocity of ith individual, c_1 and c_2 are cognitive and social index, and φ_1 and φ_2 are random numbers between 0 and 1.

The cognitive index c_1 starts with a high magnitude $c_{1\max}$ and non-linearity reduces to $c_{1\min}$. Moreover, the social index c_2 starts with a low magnitude $c_{2\min}$ and non-linearity enhances to $c_{2\max}$ according to the following functions [22]

$$\omega(k) = \omega_{\min} + \left(\frac{iter_{\max} - k}{iter_{\max}}\right)^{\alpha} (\omega_{\max} - \omega_{\min}) \tag{9.50}$$

$$c_1(k) = c_{1\min} + \left(\frac{iter_{\max} - k}{iter_{\max}}\right)^{\beta} (c_{1\max} - c_{1\min}) \tag{9.51}$$

$$c_2(k) = c_{2\max} + \left(\frac{iter_{\max} - k}{iter_{\max}}\right)^{\gamma} (c_{2\min} - c_{2\max}) \tag{9.52}$$

$$C(\phi) = \frac{2}{\left|2 - \phi - \sqrt{\phi^2 - 4\phi}\right|} \quad \text{where} \;\; 4.1 \le \phi \le 4.2 \tag{9.53}$$

where $iter_{\max}$ is the maximum iteration and α, β and γ are constant rates.

To determine the optimal mixture of α, β and γ, overall combinations must be analyzed ad c_1 is cognitive parameter (acceleration coefficient) and c_2 is Social parameter (acceleration coefficient). It is considered that:

$$\alpha, \beta, \gamma \in \{0, 0.5, 1, 1.5, 2\} \tag{9.54}$$

There are 5^3 feasible combinations for the indexes of α, β and γ. These three indexes have many feasible magnitudes, but it may not be possible to implement the experiments of all combinations. Thus, to sample a small subset of this large number of tests, an orthogonal design method will be employed. Details of the orthogonal way and its utilization have been explained in [23]. The following is an $L_{25}(5^6)$ orthogonal array that can deal with at most six variables in five feasible magnitudes with 25 tests. Instead of 5^3 feasible combinations, one only requires to implement 25 tests to find optimal combination of α, β and γ.

$$L_{25}(5^6) = \begin{bmatrix} 1 & 1 & 1 & 1 & 1 & 1 \\ 1 & 2 & 2 & 2 & 2 & 2 \\ 1 & 3 & 3 & 3 & 3 & 3 \\ 1 & 4 & 4 & 4 & 4 & 4 \\ 1 & 5 & 5 & 5 & 5 & 5 \\ 2 & 1 & 2 & 3 & 4 & 5 \\ 2 & 2 & 3 & 4 & 5 & 1 \\ 2 & 3 & 4 & 5 & 1 & 2 \\ 2 & 4 & 5 & 1 & 2 & 3 \\ 2 & 5 & 1 & 2 & 3 & 4 \\ 3 & 1 & 3 & 5 & 2 & 4 \\ 3 & 2 & 4 & 1 & 3 & 5 \\ 3 & 3 & 5 & 2 & 4 & 1 \\ 3 & 4 & 1 & 3 & 5 & 2 \\ 3 & 5 & 2 & 4 & 1 & 3 \\ 4 & 1 & 4 & 2 & 5 & 3 \\ 4 & 2 & 5 & 3 & 1 & 4 \\ 4 & 3 & 1 & 4 & 2 & 5 \\ 4 & 4 & 2 & 5 & 3 & 1 \\ 4 & 5 & 3 & 1 & 4 & 2 \\ 5 & 1 & 5 & 4 & 3 & 2 \\ 5 & 2 & 1 & 5 & 4 & 3 \\ 5 & 3 & 2 & 1 & 5 & 4 \\ 5 & 4 & 3 & 2 & 1 & 5 \\ 5 & 5 & 4 & 3 & 2 & 1 \end{bmatrix} \tag{9.55}$$

9.4.1 Fuzzy Decision Making

When solutions according to the extracted Pareto-optimal set are determined by MOPSO-NTVE method, it needs to select one of them for applying [24]. A linear membership equation is assumed for each of the target functions [12]. The membership equation is verified as bellow [25]

$$\chi_i = \begin{cases} 1, & OF_i \le OF_i^{\min} \\ \frac{OF_i^{\max} - OF_i}{OF_i^{\max} - OF_i^{\min}} & OF_i^{\min} < OF_i < OF_i^{\max} \\ 0 & OF_i \ge OF_i^{\max} \end{cases} \tag{9.56}$$

for minimized target functions and

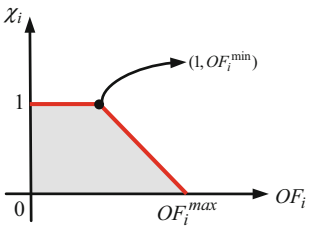

Fig. 9.11 Linear membership equation

$$\chi_i = \begin{cases} 0, & OF_i \le OF_i^{\min} \\ \frac{OF_i - OF_i^{\max}}{OF_i^{\max} - OF_i^{\min}} & OF_i^{\min} < OF_i < OF_i^{\max} \\ 1 & OF_i \ge OF_i^{\max} \end{cases} \tag{9.57}$$

for maximized target functions. Where $OF_i^{\min}$ and $OF_i^{\max}$ are the minimum and the maximum magnitude of ith target function among total non-dominated solutions, respectively. The membership equation χ is changed between 0, 1. Where $\chi = 0$ demonstrates the incompatibility of the solution with the set, while $\chi = 1$ presents full compatibility. Figure 9.11 shows a typical structure of the membership equation.

For each non-dominated solution k, the normalized membership equation χ^k is extracted as:

$$\chi^k = \frac{\sum_{i=1}^{N_{ob}} \chi_i^k}{\sum_{k=1}^{M} \sum_{i=1}^{N_{ob}} \chi_i^k} \tag{9.58}$$

where M and N_{ob} are the number of non-dominated solutions and target functions. The function χ^k can be stated as a membership function of non-dominated solutions in a fuzzy set, where the solution having the maximum membership in the fuzzy collection is assumed as the best compromise solution.

9.5 Implementation

MOPSO-NTVE algorithm is applied to determine optimal reactive plan. A decision making method according to FDM algorithm is followed to determine the best solution from the collection of Pareto-solutions created by MOPSO-NTVE technique. Details of the solution synthesis are given in Figs. 9.12, 9.13 and 9.14. For this purpose, an initial population of MPSO-NTVE is randomly produced. For each particle, AC-OPF is directed and STC and V_D are calculated. Then, the investment cost is gained. The calculation is repeated until the stopping condition is obtained. As shown in Fig. 9.15, in the RPM problem codification, each chromosome is

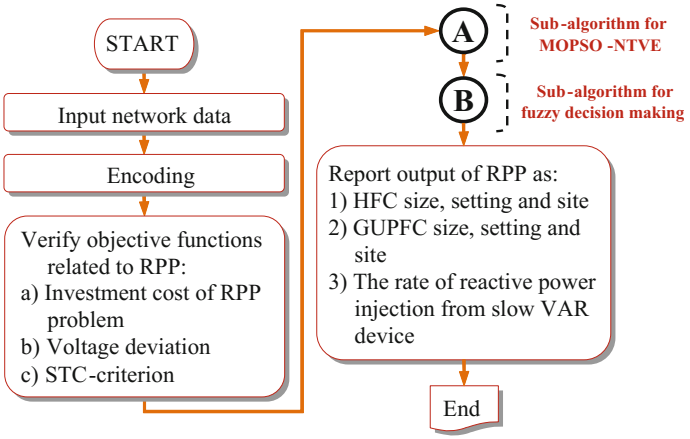

Fig. 9.12 Flowchart of the proposed RPP

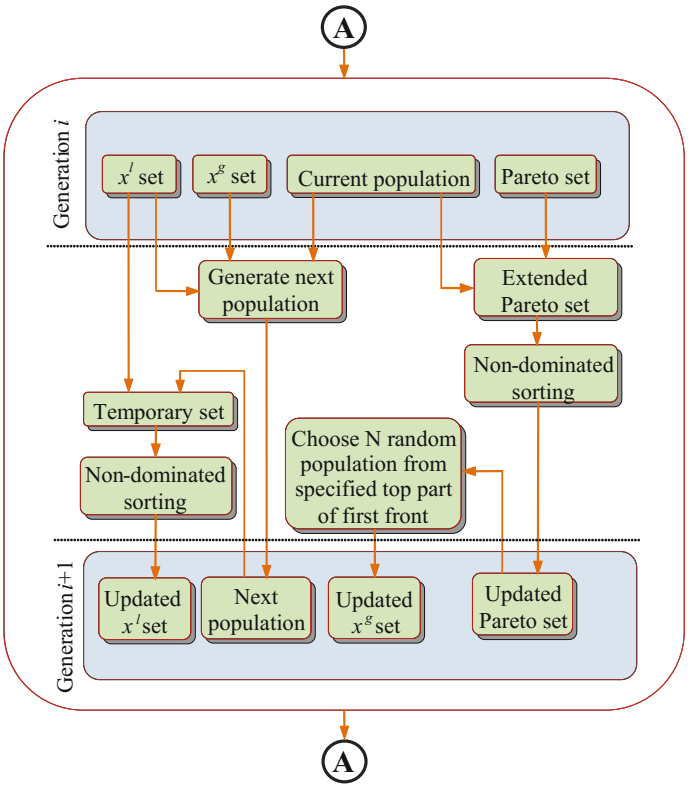

Fig. 9.13 Sub-algorithm of *A* for design procedure delineated in Fig. 9.12

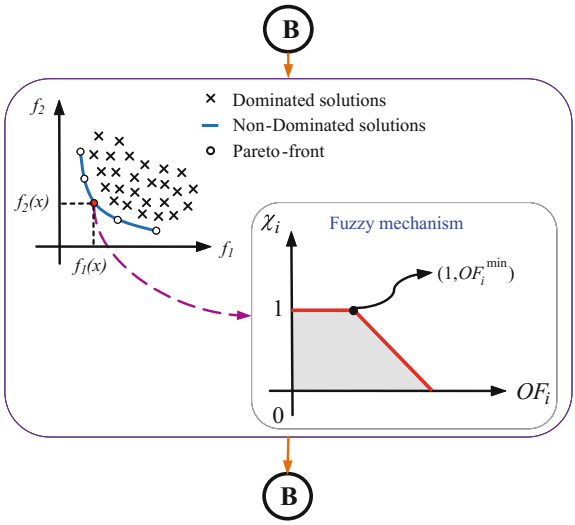

Fig. 9.14 Sub-algorithm of *B* for design procedure delineated in Fig. 9.12

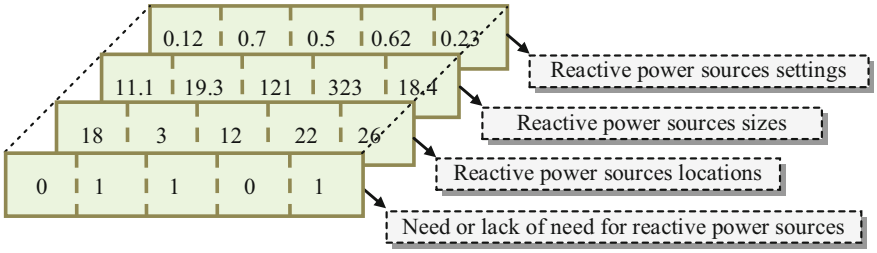

Fig. 9.15 Simple codification for RPP problem

formed from four parts of number, location, size and settings of the candidate VAR devices to be installed.

The proposed management method is implemented on a test system. The test grid employed in this work is a part of the American electric power system, AEP, applied in the Midwest in the early 1960s and is better identified as IEEE 57-node test system. The system data are available in MATPOWER toolbox [22]. The basic configuration of the test system is depicted in Fig. 9.16. The network as shown in Fig. 9.16 includes of 57 buses, 7 generators, and 80 lines. The generators are placed at nodes 1, 2, 3, 6, 8, 9, and 12. The voltage constraints are adjusted between 0.94 and 1.06 p.u.

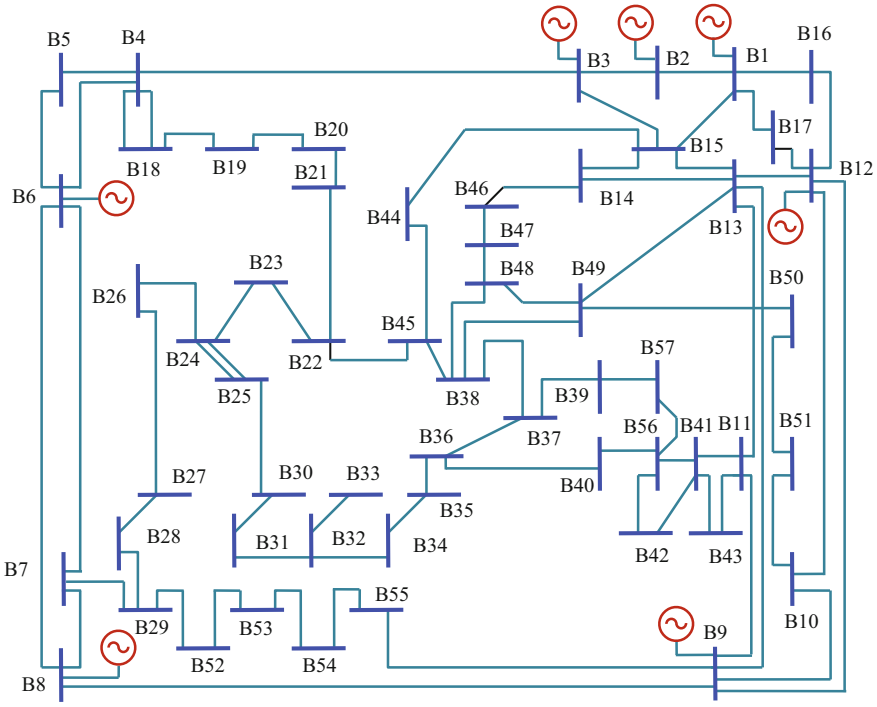

Fig. 9.16 IEEE 57-bus system

The constraints have been enforced based on Eq. (9.59):

$$\text{Evaluation Function} = \text{Objective Function} + \alpha(\text{Constraints Violations}) \quad (9.59)$$

where α is a large value and constraint violations are analyzed as the aggregate of the absolute magnitudes of all deviations. The solution will end up with the least cost selection without violating limitations. Also, discrete variables have been encoded based on "*ceil*" operators.

To analyze the effect of different FACTS tools on the power system operation, the following scenarios are studied:

- Framework 1: Slow VAR device allocation.
- Framework 2: Slow VAR device with HFC allocation.
- Framework 3: Slow VAR device with GUPFC allocation.

The performance of two frameworks is evaluated on the test system. For this purpose, the steps of the RPP problem (as given in Fig. 9.12) are performed. The Pareto-optimal archive obtained by MOPSO-NTVE algorithm in two-dimensional and three-dimensional target functions is depicted in Figs. 9.17, 9.18 and 9.19. It is observed that the gained solutions are distributed in the area, except some discontinuity, created by the discrete decision parameters. The trade-offs represented in

Figs. 9.17, 9.18 and 9.19 can help the decision maker to choose appropriate reference membership magnitudes.

A decision making approach by employing FDM theory is followed to determine the best solution as new lines from the collection of Pareto-solutions gained by MOPSO-NTVE method. FDM is used to choose size and site of the reactive power sources. Complete results related to two frameworks and four optimization methods, MOPSO, MOPSO-TVIW, MOPSO-TVAC and MOPSO-NTVE are tabled in Table 9.1.

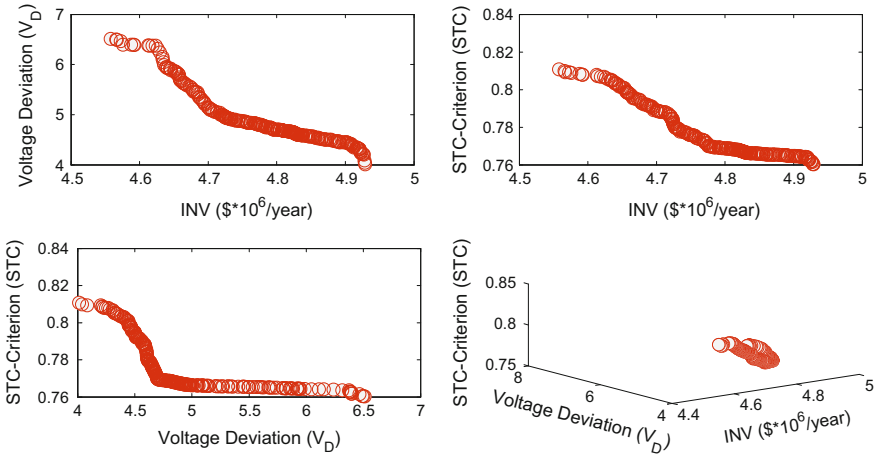

Fig. 9.17 The Pareto archive in two-dimensional and three-dimensional objective area based on framework 1

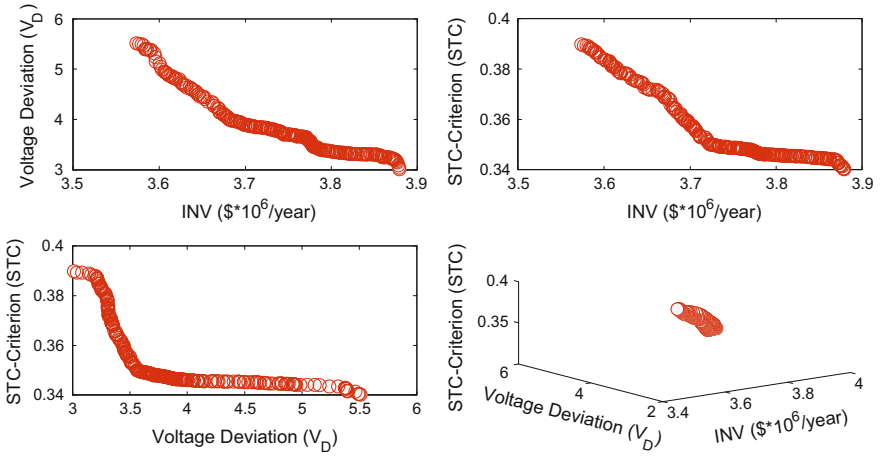

Fig. 9.18 The Pareto archive in two-dimensional and three-dimensional objective area based on framework 2

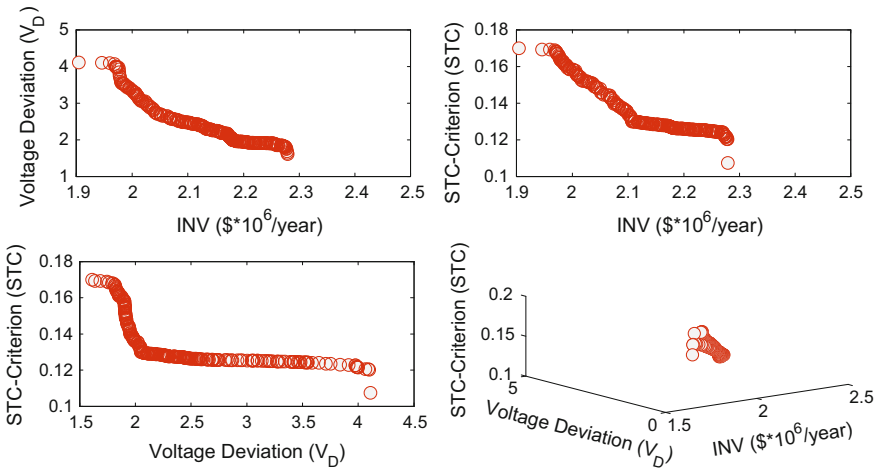

Fig. 9.19 The Pareto archive in two-dimensional and three-dimensional objective area based on framework 3

Table 9.1 Location, size and setting of reactive power sources added to network in frameworks under different solution methods

	Framework 1	Framework 2	Framework 3		
	Slow VAR devices MVAr (bus)	Slow VAR devices MVAr (bus)	HFC MVAr (location)	Slow VAR devices MVAr (bus)	GUPFC MVAr (location)
MOPSO	Q_{16} = 423.57 Q_4 = 355.56 Q_{46} = 436.56 Q_{21} = 365.56 Q_{49} = 367.97 Q_{39} = 314.56 Q_{22} = 431.56 Q_{11} = 478.03 Q_{32} = 434.67	Q_{14} = 476.56 Q_{19} = 523.56 Q_{35} = 437.67 Q_{55} = 456.73	33.34 (13-9)	Q_{11} = 475.23 Q_{53} = 478.25	13.26 (24-25, 24-23)
MOPSO-TVIW	Q_{41} = 414.76 Q_{57} = 432.45 Q_{39} = 421.45 Q_{43} = 431.56 Q_{44} = 476.67 Q_{14} = 365.76 Q_{50} = 432.67 Q_{12} = 391.67	Q_{48} = 394.67 Q_{56} = 512.56 Q_{43} = 476.56 Q_{30} = 456.65	32.9788 (22-21)	Q_{27} = 487.67 Q_{10} = 421.78	12.6786 (45-44, 45-38)
MOPSO-TVAC	Q_{18} = 409.65 Q_{46} = 434.74 Q_{50} = 446.76 Q_{49} = 346.76 Q_{39} = 476.65 Q_{41} = 421.76 Q_{56} = 365.74 Q_{31} = 418.76	Q_{11} = 535.87 Q_{35} = 465.76 Q_{32} = 421.85 Q_7 = 365.87	32.6457 (23-22)	Q_{57} = 353.64 Q_{20} = 365.87	11.6543 (29-28, 29-52)

(continued)

Table 9.1 (continued)

	Framework 1	Framework 2	Framework 3		
	Slow VAR devices MVAr (bus)	Slow VAR devices MVAr (bus)	HFC MVAr (location)	Slow VAR devices MVAr (bus)	GUPFC MVAr (location)
MOPSO-NTVE	Q_4 = 529.32 Q_{20} = 440.84 Q_{46} = 377.67 Q_{50} = 457.34 Q_{38} = 401.83 Q_{24} = 277.65 Q_{43} = 357.67 Q_{53} = 401.86	Q_{21} = 163.75 Q_{14} = 189.78 Q_{11} = 163.75 Q_{33} = 189.78	27 (49-38)	Q = 229.32 Q_{40} = 340.84	10 (15-13, 15-14)

Table 9.2 Frameworks results

	Solution methods	RPM cost (INV) ($\$ \times 10^6$/year)	Voltage deviation (V_D)	STC-criterion (STC)
Framework 1	MOPSO	4.9560	5.3219	0.7832
	MOPSO-TVIW	4.8598	5.0032	0.7755
	MOPSO-TVAC	4.7767	4.9821	0.7743
	MOPSO-NTVE	4.7257	4.9532	0.76432
Framework 2	MOPSO	4.0932	4.3217	0.3689
	MOPSO-TVIW	3.9517	4.2345	0.3578
	MOPSO-TVAC	3.8544	4.1234	0.3521
	MOPSO-NTVE	3.7713	3.9865	0.3456
Framework 3	MOPSO	2.9886	2.6422	0.1789
	MOPSO-TVIW	2.8361	2.5432	0.1675
	MOPSO-TVAC	2.3361	2.4321	0.1298
	MOPSO-NTVE	2.0085	2.3456	0.1234

To identify the advantage of the presented method, results of frameworks 1 and 2 in four solution methods are compared and tabled in Table 9.2. As shown in this table, RPP cost (INV) for framework 1 is: 4.9560, 4.8598, 4.7767 and 4.7257 and, for framework 2 it is: 4.0932, 3.9517, 3.8544 and 3.7713 and, for framework 3 it is: 2.9886, 2.8361, 2.3361 and 2.0085. RPP cost in framework 3 has 39.69, 41.64, 51.09 and 57.49% decrease compared to framework 1 and, 26.98, 28.23, 39.39 and 46.74% decrease compared to framework 2. This economic perspective of the presented way reveals priority of the obtained optimal configuration in framework 3 and the advantages of GUPFC than HFC and capacitor banks. From the viewpoint of voltage deviation (V_D) and STC-criterion, these two indices in framework 2 are significantly improved than the framework 1 in each four scenarios as displayed in Table 9.2.

Simulation test is applied for different discount rates to evaluate robustness of the proposed RPP problem. As shown in Table 9.3 twelve cases, C_1 to C_{12}, are studied. All the parameters for three discount rates (r_T = 5, 10 and 20%) and three

Table 9.3 Considered cases

Case	Discount rate (%)	Solution methods
C.1	$r_T = 5$	MOPSO
C.2	$r_T = 5$	MOPSO-TVIW
C.3	$r_T = 5$	MOPSO-TVAC
C.4	$r_T = 5$	MOPSO-NTVE
C.5	$r_T = 10$	MOPSO
C.6	$r_T = 10$	MOPSO-TVIW
C.7	$r_T = 10$	MOPSO-TVAC
C.8	$r_T = 10$	MOPSO-NTVE
C.9	$r_T = 20$	MOPSO
C.10	$r_T = 20$	MOPSO-TVIW
C.11	$r_T = 20$	MOPSO-TVAC
C.12	$r_T = 20$	MOPSO-NTVE

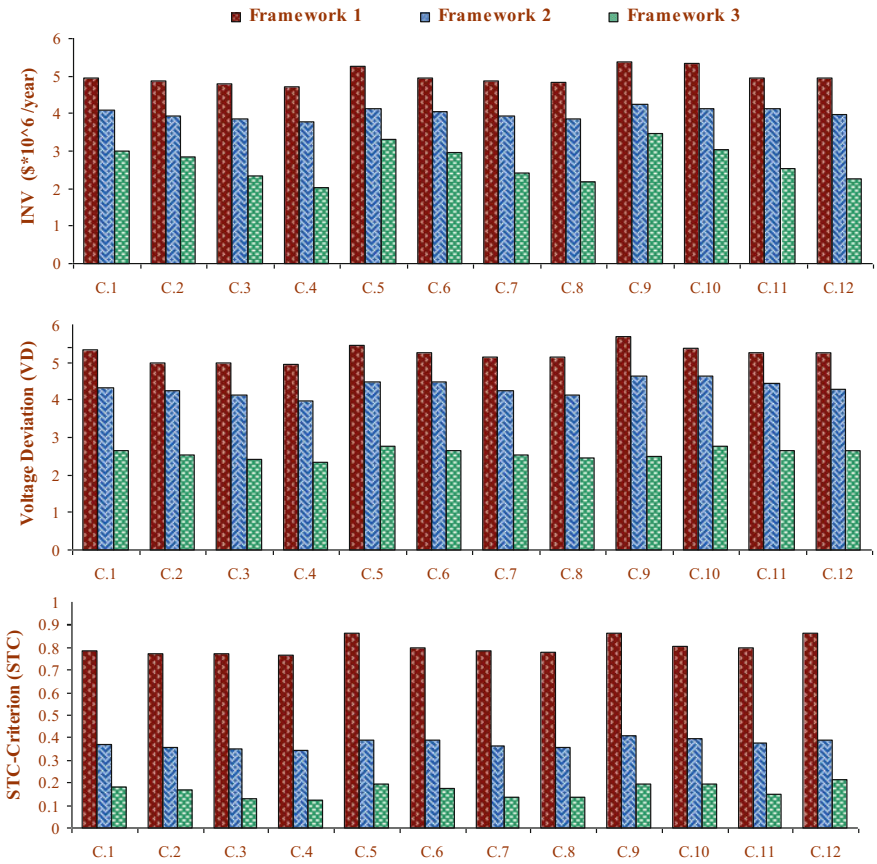

Fig. 9.20 Comparison of the performances

scenarios have been extracted, as depicted in Fig. 9.20. Results of both frameworks will change by increasing or decreasing the discount rate, but framework 3 has the best results and low changes than the nominal value of discount rate and achieves good robust performance.

9.6 Conclusion

An attempt has been made in this chapter to study solving RPP problem while HFC and GUPFC are involved in power system. A suitable model to compute reactive power that has to be injected by HFC and GUPFC is imported in the solution procedure. Multi-objective PSO-NTVE algorithm is employed and, from a decision maker perspective; the FDM method is used to define solutions by considering all attributes from the set of Pareto-solutions. The presented solution procedure is implemented on the IEEE 57-bus system as the first attempt for RPP. A comparative survey confirms that the presented management algorithm significantly improves the cost related to RPP.

The results show that inclusion of the reactive power capability of HFC and GUPFC can improve voltage stability and voltage profile. The obtained results for various scenarios reveal that this planning method is a useful management tool for solving RPP issue. The presented planning method permits the power system designers to modify the structure of the system to obtain the best optimal program for the expanded system. Simultaneous planning of reactive power expansion with the presence of capacitor banks and FACTS devices instead of separate planning can be led to more economic, applicable and optimal scheme in a power network.

References

1. H. Shayeghi, M. Ghasemi, FACTS Devices Allocation Using a Novel Dedicated Improved PSO for Optimal Techno-Economic Operation of Power System, Journal of Operation and Automation in Power Engineering, 1 (2), 2013.
2. A. Rabiee, M. Vanouni, M. Parniani, Optimal Reactive Power Dispatch for Improving Voltage Stability Margin Using a Local Voltage Stability Index, Energy Conversion and Management, 59:66-73, 2012.
3. M. Mahfouz, M.A. El-Sayed, Static Synchronous Compensator Sizing for Enhancement of Fault Ride-through Capability and Voltage Stabilization of Fixed Speed Wind Farms, IET Renewable Power Generation, 8 (1):1-9, 2014.
4. R.A. Hooshmand, R. Hemmati, M. Parastegari, Combination of AC Transmission Expansion Planning and Reactive Power Planning in the Restructured Power System, Energy Conversion and Management, 55:26-35, 2012.
5. I.P. Abril, J.A.G. Quintero, VAR Compensation by Sequential Quadratic Programming. IEEE Transactions on Power Systems, 18 (1):36-41, 2003.

6. T. Akbari, A. Rahimikian, A. Kazemi, A Multi-Stage Stochastic Transmission Expansion Planning Method, Energy Conversion and Management, 52 (8):2844-2853, 2011.
7. E. Ghahremani, I. Kamwa, Optimal Placement of Multiple-Type FACTS Devices to Maximize Power System Loadability Using a Generic Graphical User Interface, IEEE Transactions on Power Systems, 28 (2):764-778, 2013.
8. H. Shayeghi, M. Ghasemi, FACTS Devices Allocation Using a Novel Dedicated Improved PSO for Optimal Techno-Economic Operation of Power System, Journal of Operation and Automation in Power Engineering, 1 (2):124-135, 2013.
9. J. Pourhossein, G. Gharehpetian, S. Fathi, Static Inter-Phase Power Controller (SIPC) Modeling for Load Flow and Short Circuit Studies, Energy Conversion and Management, 64:145-151, 2012.
10. S.A.N. Niaki, R. Iravani, M. Noroozian, Power Flow Model and Steady-State Analysis of the Hybrid Flow Controller, IEEE Transactions on Power Delivery, 23 (4):2330-2338, 2008.
11. H. Shayeghi, Y. Hashemi, Technical-Economic Analysis of Including Wind Farms and HFC to Solve Hybrid TNEM-RPM Problem in the Deregulated Environment, Energy Conversion and Management, 80:477-490, 2014.
12. A. Lashkar Ara, A. Kazemi, S. Nabavi Niaki, Multiobjective Optimal Location of FACTS Shunt-Series Controllers for Power System Operation Planning, IEEE Transactions on Power Delivery, 27 (2):481-490, 2012.
13. Y. Hashemi, H. Shayeghi, B. Hashemi, Attuned Design of Demand Response Program and M-FACTS for Relieving Congestion in a Restructured Market Environment, Frontiers in Energy, 9:1-15, 2015.
14. B.S. Rao, K. Vaisakh, Multi-Objective Adaptive Clonal Selection Algorithm for Solving Optimal Power Flow Considering Multi-Type FACTS Devices and Load Uncertainty, Applied Soft Computing, 23:286-297, 2014.
15. Fardanesh B, Optimal utilization, sizing, and steady-state performance comparison of multiconverter VSC-based FACTS controllers. IEEE Transactions on Power Delivery, 19 (3):1321-1327. doi:10.1109/TPWRD.2004.829154, 2004.
16. K. Habur, D. OLeary, FACTS-Flexible Alternating Current Transmission Systems-for Cost Effective and Reliable Transmission of Electrical Energy, Siemens-World Bank Document-Final Draft Report, Erlangen, 2004.
17. M. Eghbal, N. Yorino, E. El-Araby, Y. Zoka, Multi-Load Level Reactive Power Planning Considering Slow and Fast VAR Devices by Means of Particle Swarm Optimization, IET Generation, Transmission & Distribution, 2 (5):743-751, 2008.
18. G. Yesuratnam, D. Thukaram, Congestion Management in Open Access Based on Relative Electrical Distances Using Voltage Stability Criteria, Electric Power Systems Research, 77 (12):1608-1618, 2007.
19. C. Coello, G. Lamont, D. Veldhuizen, Evolutionary Algorithms For solving Multi-Objective Problems, Springer, 2007.
20. F. Gunes, U. Ozkaya, Multiobjective FET Modeling Using Particle Swarm Optimization Based on Scattering Parameters with Pareto Optimal Analysis, Turk J. Elec Eng. & Comp. Sci., 20 (3):353-365, 2012.
21. A. Kavousi Fard, T. Niknam, Multi-Objective Probabilistic Distribution Feeder Reconfiguration Considering Wind Power Plants, International Journal of Electrical Power & Energy Systems, 55:680-691, 2014.
22. C. Ko, Y. Chang, C. Wu, A PSO Method with Nonlinear Time Varying Evolution for Optimal Design of Harmonic Filters, IEEE Transactions on Power Systems, 24 (1):437-444, 2009.
23. Y. Leung, Y. Wang, An Orthogonal Genetic Algorithm with Quantization for Global Numerical Optimization, IEEE Transactions on Evolutionary Computation, 5 (1):41-53, 2001.

24. A. Mazza, G. Chicco, A. Russo, Optimal Multi-Objective Distribution System Reconfiguration with Multi Criteria Decision Making-Based Solution Ranking and Enhanced Genetic Operators, International Journal of Electrical Power & Energy Systems, 54:255-267, 2014.
25. S. Christa, P. Venkatesh, Multi-Objective Optimization Problem for the Thyristor Controlled Series Compensators Placement with Multiple Decision-Making Approaches, European Transactions on Electrical Power, 23 (2):249–269, doi:10.1002/etep.658, 2011.